

## DEEP HST/ACS PHOTOMETRY OF THE M81 HALO

PATRICK R. DURRELL

Department of Physics & Astronomy, Youngstown State University, Youngstown, OH 44555; prdurrell@ysu.edu

ATA SARAJEDINI

Department of Astronomy, University of Florida, Gainesville, FL 32611

RUPALI CHANDAR

Department of Physics & Astronomy, University of Toledo, Toledo, OH 43606

*Astrophysical Journal, in press*

### ABSTRACT

We present a deep color-magnitude diagram for individual stars in the halo of the nearby spiral galaxy M81, at a projected distance of 19 kpc, based on data taken with the *Advanced Camera for Surveys* on the *Hubble Space Telescope* (*HST*). The CMD reveals a red giant branch that is narrow and fairly blue, and a horizontal branch that has stars that lie mostly redward of the RR Lyrae instability strip. We derive a mean metallicity of  $[M/H] = -1.15 \pm 0.11$  and age of  $9 \pm 2$  Gyr for the dominant population in our field, from the shape of the red giant branch, the magnitude of the red clump, and the location of the red giant branch bump. We compare our metallicity and age results with those found previously for stars in different locations within M81, and in the spheroids of other nearby galaxies.

*Subject headings:* galaxies:halos, galaxies:stellar content,galaxies: spiral,galaxies:individual(M81)

### 1. INTRODUCTION

Spheroidal stellar populations, such as elliptical galaxies and the halos and bulges of spiral galaxies, contain a significant fraction of all stars in the local universe. The ages and metallicities of halo stars in these galaxies provide some of the most important observational clues to the formation and earliest evolution of galaxies, whether through studies of globular star clusters (GCs) or, in more nearby galaxies, the individual halo stars. Below, we broadly summarize what is currently known about the ages and metallicities of stars in the spheroids of nearby galaxies.

The spheroid of the Milky Way has two components, a centrally concentrated bulge composed of more metal-rich stars, and an extended, lower density halo consisting of more metal-poor stars. The halo of the Galaxy shows substructure, with (at least) two chemically distinct components. Stars of the ‘inner halo’ have a mean  $[Fe/H] \sim -1.6$  (e.g., Ryan & Norris 1991; Allende Prieto et al. 2006; Ivezić et al. 2008), while stars in the ‘outer halo’ ( $R > 15$  kpc) are more metal-poor, with a mean  $[Fe/H] \sim -2.2$  (Carollo et al. 2007). The halo also contains many stellar streams and tidal debris that are probably the remnants of previously accreted satellite galaxies (e.g., Newberg et al. 2002; Yanny et al. 2003; Jurić et al. 2008; Smith et al. 2009; Newberg et al. 2009; Klement et al. 2009, and references therein). The globular clusters in the Galaxy have a weak metallicity gradient inside  $\gtrsim 10$  kpc, with no such trend apparent beyond 10 kpc out to the most distant cluster located at  $\approx 120$  kpc (Zinn 1985; Harris 2001). The stars and GCs in the halo of the Milky Way appear to be mostly old, with ages between 11 and 13 Gyr (Carollo et al. 2007; Marin-Franch et al. 2009), indicating that the dominant

era of accretion in the Milky Way took place soon after formation (Hammer et al. 2007).

Detailed studies of the stars in M31 suggest that this galaxy has had a more active, recent accretion history when compared with the Milky Way. M31 has a markedly metal-rich inner spheroid component (e.g., Mould & Kristian 1986; Durrell et al. 2001; Brown et al. 2003; Kalirai et al. 2006; Gilbert et al. 2007) that is dominated by substructure (Ferguson et al. 2002; Ibata et al. 2007; Richardson et al. 2008). M31 accreted a relatively massive satellite galaxy only  $\sim 1$  Gyr ago (Font et al. 2006; Fardal et al. 2006, 2007, 2008), and has had other many more minor interactions (McConnachie et al. 2009) as well. Deep images taken with the *HST*, which reach below the main sequence turnoff region for ancient stars in M31, indicate the presence of metal-rich, intermediate age stars ( $\approx 6 - 10$  Gyr) in fields located at de-projected distances of 11, 20, and 35 kpc, with a larger contribution from older, more metal-poor stars increasing at larger distances (Brown et al. 2003, 2006, 2007, 2008).

Beyond  $\sim 30$  kpc and extending out to at least  $\sim 160$  kpc, the halo of M31 is dominated by metal-poor stars with  $[Fe/H] \sim -1.5$  (Irwin et al. 2005; Guhathakurta et al. 2006; Kalirai et al. 2006; Chapman et al. 2006), and this component too has copious substructure (Ibata et al. 2007; McConnachie et al. 2009). Little is known about the ages of these stars except for the recent work of Mackey et al. (2009) who studied the M31 GC MGC1, which is located at a projected galactocentric distance of  $\sim 120$  kpc. The CMD of this cluster reveals a metal abundance of  $[M/H] \sim -2.3$  and a horizontal branch morphology that is consistent with those of Milky Way GCs at this metal abundance,

suggesting a similar age.

Studies of stars in the spheroids of several more distant elliptical galaxies suggest that metal-rich stars dominate out quite far, probably to at least  $10\text{--}15R_{\text{eff}}$ . NGC 5128 has a largely metal-rich population at radii of  $8\text{--}33$  kpc (Harris et al. 1999; Harris & Harris 2000, 2002). Even further out, an analysis of the colors of RGB stars, which are sensitive to metallicity, and the colors and luminosities of the AGB bump and the RC, which are sensitive to both metallicity and age, suggests that stars in NGC 5128 at  $R \sim 38$  kpc have largely intermediate to old ages, with  $8 \pm 3$  Gyr (Rejkuba et al. 2005). The halos of NGC 3377 and NGC 3379 have a wide range of metallicity, with a significant fraction of metal-rich stars, although metal-poor stars begin to dominate the spheroid of NGC 3379 beyond  $\approx 12R_{\text{eff}}$ . The lack of stars brighter than the RGB suggests that NGC 3377 and NGC 3379 contain few young, bright AGB stars (Harris et al. 2007a,b). Like NGC 3379, a dominant population of metal-poor stars have been found in the spheroid of the edge-on spiral galaxy NGC 891 (Rejkuba et al. 2009).

M81 is an earlier-type spiral (Sab) than either the Milky Way or M31. However, studies of the resolved stars in the outskirts of M81 have already shown that it too is a complex mix of stellar populations. Tikhonov et al. (2005) used 9 archival WFPC2 images of M81 to show that the number density of RGB and AGB stars decreases with galactocentric radius, eventually flattening out at a (deprojected distance) of  $\sim 25$  kpc. They attribute the stars interior to this as part of the thick disk, and stars beyond this as part of the halo. CMDs of fields interior to 25 kpc reveal relatively young stars (Williams et al. 2009; Dalcanton et al. 2009), and older RGB stars with a relatively large range in metallicity ( $-1 < [M/H] < 0$ ; Mouhcine et al. 2005, Williams et al. 2009). These stars are likely located in the disk, either thin or thick, of M81. More recently, Barker et al. (2009) found a flattening of the stellar density profile beyond  $\sim 20$  kpc (deprojected) from M81, with more metal-poor stars ( $[M/H] \sim -1.1$ ) than in the interior fields, again indicating that the halo dominates at these distances. The only constraint on the *ages* of stars in the halo of M81 comes from the measurement of absorption line strengths in globular clusters, which suggest ages that are indistinguishable from the GCs in the Galaxy, within the significant uncertainties ( $\approx 3\text{--}4$  Gyr) (Schroder et al. 2002).

In this work, we study the metallicities and ages of stars in a field in M81 that lies at a projected distance of 19 kpc, using observations taken with the Advanced Camera for Surveys on *HST*. These data are among the deepest available for a portion of M81. The rest of this paper is organized as follows: Section 2 presents the data and reduction; Section 3 presents the CMD for our field and discusses general features; Section 4 presents a new determination of the distance to M81 from the tip of the RGB, and averages this with previous distance determinations to give our adopted value; Section 5 discusses the red clump, and Section 6 presents an estimate of the metallicities and ages of stars in our M81 field. Section 7 presents some new results on a small population of blue stars discovered in our field, and Section 8 discusses the results in terms of the formation of M81, as well as our main conclusions.

## 2. OBSERVATIONS AND REDUCTIONS

Observations of M81 were obtained with the Wide Field Channel (WFC) of the Advanced Camera for Surveys (ACS) on-board the *HST*, for program GO-10604 (PI: Sarajedini). A single ACS/WFC pointing covering  $\approx 3.4' \times 3.4'$  was centered at  $\alpha = 9^{\text{h}}53^{\text{m}}03^{\text{s}}20$ ,  $\delta = +68^{\circ}52'03.6''$  (J2000.0), at a projected distance of  $18'$  from the center of M81, or 19 kpc at the adopted distance of 3.7 Mpc (see Section 4).

The specific pointing was chosen to lie along the southwestern semi-minor axis, beyond the radius suggested as the edge of M81's thick disk (Tikhonov et al. 2005), where the surface brightness of M81 is still high enough that we can determine a meaningful metallicity distribution from RGB stars. Figure 1a shows the location of our ACS pointing. It also shows the WFPC2 field studied by Mouchine et al. (2005), which falls on the edge of the suggested thick disk in M81, at a projected distance of  $12.8'$  (14 kpc) from the center of M81. Figure 1b shows our pointing superposed on HI contours from Yun et al. (1994); while our field is outside of M81's purported thick disk (at a deprojected distance of 30–34 kpc), it still lies along the line-of-sight with some of the many HI filaments that exist outside M81's optical disk (Yun et al. 1994). While some of this HI has been tidally stripped from M81 by encounters with M82 and NGC 3077, probably  $\approx 220\text{--}280$  Myr ago (Yun 1999), velocities of the HI towards our field are consistent with rotation of the M81 disk (M.Yun, private communication).

Our field was observed on 2005 Sept. 11–13 for 5 orbits (2 images per orbit) in the F606W filter and 9 orbits (2 images per orbit) in the F814W filter, using a standard 4-point dither pattern. Each individual exposure had an exposure time of 1247s, leading to a total exposure time of 12470s in the F606W filter, and 22446s in the F814W filter. We retrieved the pipeline flatfielded images from the *HST* archive as well as the pipeline-processed multidrizzled combined images from subsets of the data.

Photometry was performed with the ACS module of the DOLPHOT software package (Dolphin 2000), which is specifically designed for point-source photometry of objects in the individual FLT images, which were taken directly from the *HST* archive. Object detection and photometry was performed on all exposures simultaneously, using one of our deep F814W drizzled images (derived from a subset of 8 images) as the reference frame. The DOLPHOT parameters were set to the recommended values given in the DOLPHOT User's Guide <sup>1</sup>, which includes PSF-fitting using pre-derived PSFs, as well as the calculation and application of CTE correction (Riess 2003) and aperture corrections. The instrumental magnitudes were converted to the VEGAmag *HST* photometric system by adopting the revised zeropoints (for data taken before July 4, 2006) of 26.420 for F606W and 25.536 for F814W, which differ by  $\sim 0.02\text{--}0.03$  mag from the values originally published by Sirianni et al. (2005). We refer to magnitudes in this system by their filter name ( $m_{F606W}$  and  $m_{F814W}$ ), and in cases when we need to convert to the Johnson-Cousins systems refer to the filters as  $V$  and  $I$ .

We determined the photometric completeness limits

<sup>1</sup> <http://purcell.as.arizona.edu/dolphot/>

and associated errors in our point-source photometry by adding and remeasuring 60,000 artificial stars in the ACS images. The artificial stars have a range of magnitude ( $24 < m_{F814W} < 31$ ) and color ( $-0.25 < m_{F606W} - m_{F814W} < 2.25$ ). The Pritchett interpolation function (Fleming et al. 1995)

$$f(m) = \frac{1}{2} \left( 1 - \frac{\alpha(m - m_{lim})}{\sqrt{1 + \alpha^2(m - m_{lim})^2}} \right) \quad (1)$$

was used to fit the binned completeness fractions  $f$  (= number of stars detected / number of stars added) as a function of magnitude. Here,  $\alpha$  is a parameter that measures the rate of decline of  $f(m)$  at  $m_{lim}$ , and  $m_{lim}$  is defined as the 50% completeness limit. To account for completeness variations in both color and magnitude, we used only the bluest stars ( $m_{F606W} - m_{F814W} = 0$ ) to determine the F814W completeness fraction  $f(F814W)$ , and redder stars ( $m_{F606W} - m_{F814W} > 1$ ) to derive  $f(F606W)$ . The limiting magnitude ( $f = 0.5$ ; Harris 1990) for each filter is  $m_{F606W,lim} = 29.73$  and  $m_{F814W,lim} = 28.79$ .

### 3. GENERAL FEATURES IN THE COLOR-MAGNITUDE DIAGRAM

We selected point sources in our field as follows. First, we restricted our sample to objects with a DOLPHOT category consistent with stars (OBTYP=1). Of the sources that met this criterion, only those that were measured on at least 8 of the 10 individual F606W images, and on at least 15 of the 18 individual F814W images were retained, yielding a list of 13,858 sources over the entire ACS field. To remove remaining, slightly resolved objects, we applied the following cuts:  $\chi^2 < 2$  (from the PSF fitting), and a crowding parameter CROWD  $< 0.4$  mag, where the latter rejected objects whose magnitudes are likely to be affected by neighboring sources. Finally, we kept only those objects with sharpness values within an empirically-derived hyperbolic function:  $|SHARP| < 0.01 + 0.16e^{0.46(F814W - 28)}$ . All of these criteria were chosen based on visual inspection of sources on the ACS images. The  $m_{F606W} - m_{F814W}$  versus  $m_{F814W}$  color-magnitude diagram (CMD) for the 9081 remaining objects (representing our ‘cleaned’ sample of stellar objects in the M81 field) is shown in the left panel of Figure 2, with the CMD of all objects *rejected* by the CHI/SHARP/CROWD cuts plotted in the right hand panel. The photometric errors derived from the artificial star experiments, as well as the 50% photometric completeness levels, are also plotted in the left-hand panel.

Comparison of the two plots shows that the vast majority of rejected objects do not correspond to the sequences visible in the ‘clean’ CMD, lending credence to our choice of classification criteria. We note that some true stellar sources will be removed by our somewhat stringent selection criteria, but since we are most interested in those objects with the best quality photometry, these are acceptable ‘losses’.

The cleaned CMD extends from above the tip of the first ascent red giant branch (TRGB) to one magnitude below the horizontal branch (HB). Stars on the red giant branch are older than a few Gyr. The HB has a morphology which is predominantly redward of the RR Lyrae instability strip, although we cannot unambiguously detect

an extended blue horizontal branch due to the presence of a small population of blue stars ( $m_{F606W} - m_{F814W} \sim 0$ ), which will be discussed in Section 7. In fact, the red HB resembles a red clump (RC) most commonly seen in relatively young (down to  $\approx 1$  Gyr) and/or metal-rich stellar populations. An analysis of the RGB and RC stars is presented in Section 5. There is a small but noticeable population of stars above the TRGB, likely asymptotic giant branch (AGB) stars of intermediate age ( $\sim 5$  to 10 Gyr). From the Besançon Galaxy model of Robin et al. (2003), we estimate that there should be  $\approx 7$  (foreground) stars from the Milky Way with  $21 < I < 24$  and  $1.5 < (V - I) < 4$  in our field of view, so the vast majority of stars in our M81 field in this color and magnitude range belong to M81. We will explore these populations in more detail in the upcoming sections.

## 4. DISTANCE TO M81

### 4.1. The RGB Luminosity Function

We determine the luminosity function of the RGB stars in our field by defining an ‘RGB zone’ and thereby excluding stars far from the RGB sequence. We use the  $Z=0.0001$  and  $Z=0.004$  models of Girardi et al. (2002) to provide a general guide to the shape of the RGB in both color and luminosity, after first making the models redder and bluer by 0.05 mag to accommodate photometric uncertainties; see Figure 3. However, we explicitly include stars brighter than the tip of the RGB, likely to be AGB stars, by allowing a larger range of magnitudes than the model predictions.

In Figure 4, we show the  $m_{F814W}$  luminosity function of the RGB in our field for those objects in the extraction region with  $22 < m_{F814W} < 28$ , with a bin width of 0.08, and uncertainties given by  $\sqrt{N}$ . We do not make a correction for foreground stars, because we found in §3 that these are very sparse in this direction. The red clump is clearly present at  $m_{F814W} \sim 27.8$ ; we will return to this feature in Section 5.

### 4.2. Tip of the Red Giant Branch

In order to interpret our CMD further, we need to know the distance to M81. Here, we determine the distance from the tip of the RGB (TRGB) in the  $I$ -band, which has proven to be an excellent distance indicator for metal-poor, old stellar populations (e.g., Lee et al. 1993; Sakai et al. 1996; Ferrarese et al. 2000; Bellazzini et al. 2001; McConnachie et al. 2004; Mouchine et al. 2005). Visual inspection of our CMD shows a transition in the number counts at  $m_{F814W} \sim 24.0$ , albeit with a small number of stars. While a small number of stars in the upper part of the RGB (there are  $\sim 110$  in our CMD) can lead to a possible systematic bias in the determination of  $I_{TRGB}$ , Madore & Freedman (1995) have shown that with at least  $\sim 100$  stars in the top magnitude of the RGB (as is the case for our luminosity function), such biases are expected to be small.

To derive a quantitative estimate of the location of the RGB tip, we have employed the Sobel edge-detection filter (Sakai et al. 1996) in order to find the strongest discontinuity in the bright part of our LF in Figure 4 (for the relatively small number of stars in the upper RGB, this simple edge-detection method should suffice for our purposes). Each object in the LF is modelled as

a Gaussian distribution with a dispersion equal to the expected photometric error. We use the dispersion in the mean of the individual DOLPHOT magnitudes as our photometric error. The resulting luminosity function  $\Phi(m)$  is plotted at the top of Figure 5. To determine the location of the RGB tip, we applied to this LF the edge-detection algorithm

$$E(m) = \Phi(m + \sigma(m)) - \Phi(m - \sigma(m)) \quad (2)$$

where  $\sigma(m)$  is the mean photometric error defined from our artificial star experiments (Sakai et al. 1996). The resultant response function is plotted in the bottom of Figure 5, and shows a peak at  $m_{F814W} = 24.00 \pm 0.02$ , where the small formal uncertainty reflects only the width of the Sobel function peak. Converting to the  $I$ -band via the synthetic transformations of Sirianni et al. (2005) (and using the revised zeropoints, as noted above), we find  $I_{TRGB} = 23.97 \pm 0.04$ , where we have adopted an uncertainty of 0.03 mag in the transformation from  $m_{F814W}$  to  $I$ . The true uncertainty in  $I_{TRGB}$  is almost certainly larger than that given above, since they do not include any uncertainties in the photometry itself.

The distance to M81 is determined by comparing the measured magnitude for the tip of the RGB found above with the predicted intrinsic magnitude,  $M_{I,TRGB} = -4.05 \pm 0.02$  (for  $[\text{Fe}/\text{H}] = -1.6$ ) from Rizzi et al. (2007). This predicted value is very similar to  $M_{I,TRGB} = -4.06 \pm 0.07$  (random error) derived by Ferrarese et al. (2000), and to  $M_{I,TRGB} = -4.04 \pm 0.12$  (for  $[\text{Fe}/\text{H}] = -1.7$ ) from Bellazzini et al. (2001). A comparison between observed and predicted  $M_{I,TRGB}$  magnitudes gives an observed distance modulus of  $(m-M)_I = 28.02 \pm 0.05$  for M81, or an intrinsic value of  $(m-M)_o = 27.86 \pm 0.06$  ( $d = 3.73 \pm 0.16$  Mpc), where we have assumed a foreground extinction of  $A_I = 0.16 \pm 0.04$  (using  $E(B-V) = 0.08$ ; Schlegel et al. 1998) and adopted a 0.02 uncertainty in the foreground reddening to M81. This is consistent with determinations from independent TRGB estimates and other methods, as discussed below.

#### 4.3. Previous and Adopted Distance Determinations

Several different techniques have been used previously to estimate the distance to M81, leading to distance modulus estimates that differ by approximately 0.1 mag.

The period-luminosity relationship for Cepheid variables is a robust way to determine the distance to nearby galaxies. Ferrarese et al. (2000) determined a value of  $(m-M)_o = 27.80 \pm 0.08$  for M81, based on 30 Cepheids discovered in M81 by Freedman et al. (1994), using *HST* observations. More recently, McCommas et al. (2009) determined a distance modulus of  $27.78 \pm 0.05 \pm 0.14$  based on 11 Cepheids, in good agreement with the distance determined by Ferrarese et al. Here, we adopt the McCommas et al. value as the Cepheid based distance to M81.

Estimates of the distance to M81 based on the tip of the RGB method tend to give a range of values. We found  $(m-M)_o = 27.86 \pm 0.06$  above, and Tikhonov et al. (2005) derived a mean value of  $(m-M)_o = 27.92 \pm 0.04$ , based on fields which are interior to that used here. However, Rizzi et al. (2007) derive a much shorter distance modulus of  $(m-M)_o = 27.68 \pm 0.04$  from their detection of the TRGB in an M81 disk field, and Dalcanton et al.

(2009) derived a value of  $(m-M)_o = 27.77$  from deep photometry of an ACS field in M81's disk.

For this work, we adopt a distance of  $\langle(m-M)_o\rangle = 27.80 \pm 0.08$  ( $d = 3.63 \pm 0.14$  Mpc) to M81, which is the mean value of the five distance determinations described above (4 TRGB values and the Cepheid value). The quoted error is the dispersion of the input values (each of the individual distance determinations have similar uncertainties).

#### 5. LOCATION OF THE RED CLUMP

Inspection of Figure 2 shows a well-populated horizontal branch, indicating a population of relatively old stars. While our data do not allow for a clean detection of a blue horizontal branch, the magnitude and color of the red clump (RC<sup>2</sup>) allows us to estimate the age and metallicity of the dominant stellar population in our field, as shown in the next section.

To derive the photometric properties of the RC, we use only those stars with colors in the range  $0.80 < V-I < 1.10$ ; a close-up of this part of the CMD is shown in Figure 6, along with the luminosity function of stars in this color range, where the RC is clearly visible. To derive the mean magnitude of this feature, we fit the ‘background’ LF immediately brighter and fainter than the RC as a linear function, and fit a single Gaussian to the LF once the linear background has been subtracted off. We note that the choice of bin size and the exact background fit have negligible effect on the mean magnitude determined for the RC clump. The resulting fit (and  $1\sigma$  uncertainties) yields  $I_{RC} = 27.75 \pm 0.04$ . The Gaussian width of  $\sigma_I = 0.14 \pm 0.04$ , while consistent with the expected photometric errors from the artificial star experiments, does allow for some intrinsic spread in age and/or metallicity. Given our adopted distance modulus of  $\langle(m-M)_o\rangle = 27.80 \pm 0.08$ , the I-band absolute magnitude in this region of M81 is  $M_I(\text{RC}) = -0.21 \pm 0.10$ . The location of the RC in our dataset is also consistent with the value derived by (Williams et al. 2009) for their M81 outer disk field<sup>3</sup>.

We note the presence of a small positive feature at  $I \sim 27.42 \pm 0.05$  (adopted error based on the bin size used) in the LF in Figure 6. This feature is very likely the faint signal from the RGB bump<sup>4</sup>, the location on the RGB

<sup>2</sup> Here we equate the RC with the ‘red horizontal branch’ (RHB), where the vast majority of helium-burning stars lie redward of the instability strip

<sup>3</sup> This may seem odd considering the large differences in stellar population between the two studies. Williams et al. (2009) quote  $m_{F814W,RC} = 27.792 \pm 0.002$  while we get  $m_{F814W,RC} = 27.78 \pm 0.04$ . The Williams et al. field exhibits a mean age of 2-3 Gyr and a metallicity of  $[\text{M}/\text{H}] \sim -0.7$ . In our field (see next section) we find a mean age of 9 Gyr and a  $[\text{M}/\text{H}] = -1.15 \pm 0.03$ . Our M81 field is  $\sim 6$  Gyr older and  $\sim 0.5$  dex more metal-poor than the Williams et al. field. A change of  $-0.5$  dex makes the red clump 0.15 mag brighter and a change of  $+6$  Gyr makes the red clump 0.17 mag fainter (based on Fig. 8 of Williams et al. 2009), so they offset each other resulting in a RC absolute magnitude that is essentially unchanged.

<sup>4</sup> This feature is not the AGB bump, which would be more luminous than the RC by  $\approx 1$  mag (e.g., Rejkuba et al. 2005; Williams et al. 2009). We do not see strong evidence for an AGB bump here because of the relatively low number of stars in our field. Williams et al. (2009) do see an AGB bump, because their field contains many more stars, but do not observe an RGB bump, likely because their significantly larger range of metallicities and ages washes out this feature.

where the hydrogen-burning shell crosses the discontinuity in chemical abundances remaining from the stars' convective envelope (Ferraro et al. 1999; Alves & Sarajedini 1999). The luminosity of the RGB bump depends on both the metallicity and the age of the stars, and will be used as a consistency check on our results in the next section.

## 6. MEAN METALLICITY AND AGE OF THE M81 FIELD

The absolute magnitude of the red clump, as well as the shape (slope) and location (color) of the RGB are both sensitive to the age and metallicity of the stellar population. However, the RGB is more sensitive to metallicity than to age, and the magnitude of the RC is more sensitive to age than to metallicity, so it is possible to use both features together to constrain the age and metallicity of the dominant population.

We compare the observations with the theoretical isochrones of Girardi et al. (2000), assuming scaled-solar abundance.<sup>5</sup> We first correct the colors and magnitudes using the values for reddening and distance noted above. Next, we assume an age and use the colors of RGB stars with  $M_I < -2.0$  to determine metallicity based on an interpolation within the Girardi et al. (2000) grid of theoretical isochrones with  $-2.3 \leq [M/H] \leq 0.0$ . Figure 7 shows these theoretical RGBs overplotted on our M81 CMD for an age of 9 Gyr. The  $M_I < -2.0$  magnitude range is chosen to minimize the effect of asymptotic giant branch stars on the blue side of the RGB (e.g., Sarajedini & Jablonka 2005). The resultant mean metallicity and the I-band absolute magnitude of the RC derived above,  $M_I(RC) = -0.21 \pm 0.10$ , are used in conjunction with the Girardi et al. (2000) models for the median magnitude of the red clump stars to infer the age of the population. This age estimate  $\tau$  is then used to re-determine the mean metallicity from the RGB stars and the process is repeated. This iterative procedure converges quickly and yields a mean metallicity of  $[M/H] = -1.15 \pm 0.03$  (random),  $\pm 0.11$  (systematic), where the latter value includes the influence of errors in the distance modulus and reddening. The mean age of the dominant population is then  $\langle \tau \rangle = 9 \pm 2$  Gyr, where the quoted uncertainty reflects the error in the red clump magnitude, which is the dominant source of uncertainty. The resultant metallicity distribution function (MDF) is shown in Fig. 8 wherein the fitted Gaussian profile gives a 1- $\sigma$  width of 0.39 dex in  $[M/H]$ .

The dominant signal in the MDF is due to stars around  $M_I \sim -2$  to  $\sim -3$ . The artificial star tests we have performed suggest that the mean color error at  $M_I \sim -2.4$  is 0.032 mag, which corresponds to  $\sigma_{[M/H]} \sim 0.12$  dex based on the Girardi et al. (2000) isochrones in the range  $-1.3 \leq [M/H] \leq -0.7$ . This suggests a significant fraction of

the  $\sigma_{[M/H]}$  exhibited by the MDF is due to an intrinsic range in metallicity among the M81 stars in our field. In particular, subtracting the dispersion due to errors from the measured dispersion in quadrature yields an intrinsic abundance spread of  $\sigma_{[M/H]} = 0.37$  dex.

It is also important to keep in mind that we have used scaled-solar isochrones for the determination of the MDF shown in Fig. 8. The degree to which field stars in the M81 halo are enhanced in the  $\alpha$ -capture elements is currently not known. We can estimate the effect of such an enhancement on our MDF using the formalism of Ferraro et al. (2000):

$$[M/H] = [Fe/H] + \log(0.638f_\alpha + 0.362)$$

where  $f_\alpha$  represents the factor by which the  $\alpha$ -elements are enhanced. Thus, if  $[\alpha/Fe] = +0.3$ , then  $f_\alpha = 2$  and our computed scaled-solar  $[M/H]$  values are larger than  $[Fe/H]$  by  $\sim 0.2$  dex.

We conclude this section by providing a series of consistency checks on our principle result, which is that the mean metallicity and age of stars in our M81 field are  $[M/H] = -1.15 \pm 0.11$  and  $9 \pm 2$  Gyr, respectively. First, the location of the weak RGB bump (described in the previous section) at  $I \sim 27.42 \pm 0.05$  can be used to provide an independent estimate of the age/metallicity of the M81 field stars. Indeed, the RGB bump lies above the HB/RC for primarily old, more metal-poor populations (Ferraro et al. 1999; Alves & Sarajedini 1999). From our adopted distance modulus, an assumed mean color  $(V - I) = 0.95 \pm 0.05$  and  $A_V = 0.27$ , we find  $M_{V,RGBbump} \sim 0.30 \pm 0.10$ . From the relations in Alves & Sarajedini (1999) (and adopting an additional 0.1 dex uncertainty in those relations), this translates to a metallicity  $[Fe/H] \sim -1.6 \pm 0.2$  for an old, 12 Gyr population, or a metallicity  $[Fe/H] \sim -1.3 \pm 0.2$  for a 9 Gyr population. While the uncertainties in these results are large, and the  $\alpha$  enhancement unknown, the age and metallicity derived from the RGB bump are broadly consistent with what we find from the location of the RC. A further comparison of our derived value of  $M_{I,RC}$  with predicted values presented by Rejkuba et al. (2005) (their Fig. 22; based on models by Pietrinferni et al. (2004)) are also consistent with a metal-poor population with an age of  $\sim 8$  Gyr.

As an additional check, we compare our CMD with that for the Galactic globular cluster NGC 362, studied as part of the *HST* Treasury project GO-10775 (Sarajedini et al. 2007; Marin-Franch et al. 2009). This cluster has a metallicity of  $[Fe/H] = -1.09$  (on the Carretta & Gratton (1997) scale), and an age of  $\sim 10.5$  Gyr (Marin-Franch et al. 2009), and therefore provides a good reference for our field. Figure 9 shows our M81 photometry compared with the NGC 362 fiducial sequence derived from the *HST* Treasury project data. The latter has been shifted by  $\Delta(m_{F814W}) = 13.12$  and  $\Delta(m_{F606W} - m_{F814W}) = 0.05$ . These are based on adopted values of  $(m - M)_o = 14.77$  and  $E(B - V) = 0.037$  for NGC 362 (Sarajedini 2009) and  $(m - M)_{F814W} = 27.95$  and  $E(F606W - F814W) = 0.080$  for M81. We see good agreement between the location and shape of the NGC 362 fiducial and the locus of M81 stars along the red clump and the RGB. The color distribution of M81 RGB stars is slightly bluer than the NGC 362 RGB fiducial,

<sup>5</sup> The determination of stellar metallicities for the RGB stars in our field is performed in the *HST* VEGAmag  $m_{F606W} - m_{F814W}$  CMD as this makes use of the well-determined photometric zero-points for the ACS/WFC instrument. However, the theoretical dependence of the red clump magnitude on metallicity and age is performed in the ground-based system as it requires knowledge of the median I-band RC magnitude for a population of stars, and these have only been constructed for the ground-based filters. This is unlikely to introduce a significant systematic effect because the ACS/WFC F814W passband closely matches its ground-based I-band counterpart. We also note that the RGBs of the Girardi et al. (2000) isochrones are identical to those of Marigo et al. (2008).

and is most evident within one magnitude of the M81 RGB tip. This could be due to NGC 362 being slightly more metal-rich ( $\sim 0.05$  dex) and somewhat older (1 to 2 Gyr) than the mean properties of the M81 field. Taken together, these could account for a color difference of  $\sim 0.03$  mag in  $m_{F606W} - m_{F814W}$  on the RGB.

### 7. BLUE STARS

Our CMD of the M81 halo field shows a (small) population of blue stars with  $m_{F606W} - m_{F814W} \approx 0$ , properties expected for young ( $\approx 10^8$  yr) stars, but not for the stars in the halo of a spiral galaxy. We have checked that these are genuine sources with blue colors. They are clearly point-like and not obvious background galaxies, and are scattered throughout our ACS field. We conclude that these are likely individual, young stars associated with M81. Furthermore, the rather sudden appearance of these objects at  $m_{F814W} \sim 26$  blueward of the dominant RGB suggests that these are not RGB or RC stars in M81 scattered due to large photometric errors. An overlay of metal-rich ( $Z=0.008$ ;  $[M/H] \sim -0.4$ ) isochrones from Marigo et al. (2008) onto our CMD is shown in Fig. 10, and suggests that these blue stars have ages between  $\approx 200$ -400 Myr.

What is the origin of these stars? They have colors and magnitudes similar to a stellar population seen in the CMD of an outer disk field in M81 (Figure 3 in Williams et al. 2009). Potentially then, there is a sparse outer disk in M81, which contributes a very small fraction of the stars observed in our field. If these stars are an extension of the true outer disk of M81, then the disk plane extends out  $\approx 34$ -40 kpc from M81.

A second possibility is that these stars formed in the disk of M81 or in one of its companions, and then were carried to this location along with the HI tidal debris that is coincident with our field, likely as a result of the most recent galactic interactions between M81, M82 and NGC 3077, which occurred  $\sim 220 - 280$  Myr ago (Yun 1999, see also Weisz et al. 2008).

The observed HI gas along the line-of-sight to our ACS field has a column density of only  $N_{HI} \sim 10^{20} \text{ cm}^{-2}$  (Yun et al. 1994). Recent ( $\sim 30 - 70$  Myr) star formation has been found not only in the outskirts of M81 itself (Barker et al. 2009) but also in nearby tidal dwarf galaxies such as Holmberg IX (Weisz et al. 2008; Sabbi et al. 2008), BK3N (Makarova et al. 2002), and in other nearby tidal debris (Durrell et al. 2004; Davidge 2008; Chiboucas et al. 2009; Mouhcine & Ibata 2010). However, in all of these cases, the recent star formation has occurred in areas with higher HI column densities ( $N_{HI} > 4 - 8 \times 10^{20} \text{ cm}^{-2}$ ) than that observed in our field, and is thus consistent with the lack of *recent* (i.e.  $\tau \lesssim 10^8$  yr) star formation in our field. This is also consistent with the findings of Maybhate et al. (2007), who find recent low-level star formation at levels  $N_{HI} \sim 4 \times 10^{20} \text{ cm}^{-2}$ . We note that while recent episodes of star formation in the outermost regions of late types galaxies have been observed at column densities similar to that in our field ( $\sim 10^{20} \text{ cm}^{-2}$ ; e.g. de Blok & Walter 2003; Thilker et al. 2007), we do not see evidence of this in our (small) field.

We conclude that while we do see evidence for blue stars in our field, these make only a small contribution to the stellar population in our M81 field.

### 8. DISCUSSION AND CONCLUSIONS

The main result from our analysis of a field at a (projected) distance of  $18'$  (19 kpc) from the center of M81, just beyond the suggested edge of the thick disk, is that the dominant population has a mean age of  $9 \pm 2$  Gyr and a peak metallicity of  $[M/H] = -1.15 \pm 0.11$ . Below, we discuss these results in the context of the formation history of M81, and compare with results from the spheroids of other nearby galaxies.

The color distribution of stars on the RGB in our M81 field is relatively blue and rather narrow. We derived the metallicity distribution of these RGB stars by comparing with theoretical isochrones, and find a mean  $[M/H]$  of  $-1.15$ , with an intrinsic dispersion of  $0.37$  dex as shown in Figure 8. Our field is dominated by stars that are more metal-poor than stars located closer to the center of M81; indeed, our ACS field contained the most metal-poor stars in any M81 field observed thus far. In Figure 11, we compare our MDF (for an assumed age of 9 Gyr) with that determined by Mouhcine et al. (2005) (for globular cluster-like ages;  $\sim 12$  Gyr for a field that is also along the southwest minor axis, but somewhat closer to the center of M81 with a projected distance of  $\sim 14$  kpc (see Figure 1)). While the general shape for the MDF is similar in both fields, the Mouhcine et al. field is clearly dominated by stars which are more metal-rich by  $\approx 0.4$  dex than the stars studied here (where we have already accounted for the differences in the assumed ages of the MDFs – adopting a slightly older (by  $\sim 3$  Gyr) age would effectively *decrease* the mean metallicity of our MDF by  $\sim 0.1$  dex; making the difference between the MDFs larger). This metallicity difference is not likely to be due to uncertainties in the colors or in the adopted reddening values; to match a  $0.4$  dex difference in  $[M/H]$ , our mean RGB would need to be redder by  $\sim 0.1$  in ( $m_{F606W} - m_{F814W}$ ). Similarly, the MDFs of Mouhcine et al. (2005); Mouhcine et al. (2006) are more metal-poor than the outer (thick?) disk field presented by Williams et al. (2009), a field dominated by relatively old (2/3 of stars formed more than  $\sim 8$  Gyr ago) but relatively metal-rich stars.

This sequence of declining metallicity with location indicates that either there is a strong metallicity gradient in the disk of M81, or that our field (as well as the Mouhcine et al. field) samples a different structural component of M81 than Williams et al. (2009). The markedly lower metallicity between our field and that of the outer disk of M81, combined with the relatively old ages inferred for these stars (discussed below) and the lack of (much) recent star formation, provide tentative evidence that our field is largely dominated by stars in the *halo* of M81, rather than in a thick disk.

In a recent wide-field study of bright stars in M81's outer regions Barker et al. (2009) suggest the presence of a faint, structurally distinct component surrounding M81 with a mean metallicity  $[M/H] \sim -1.1 \pm 0.3$ ; the large uncertainty is due to the rather limited part of the RGB observable in their ground-based data. This metallicity is slightly higher than (but consistent with) the value found here<sup>6</sup>. Our field is not located within the

<sup>6</sup> it is important to note that Barker et al. (2009) assumed an age of 10 Gyr; if instead they had assumed 9 Gyr as we derive here, this would increase their derived metallicity less than 0.1 dex

region surveyed by Barker et al. (2009), but lies at a de-projected distance of 34-40 kpc from M81, comparable to the distance of the fields used for their metallicity estimate. This extended component has properties similar (but not identical) to either the Milky Way thick disk or the halo, making the exact nature of this structure somewhat uncertain. Future deep observations of M81's outer regions will be needed to help establish the true nature of this feature.

We can compare the MDF that we derive for our 20 kpc field in M81 with the metallicities found for the spheroids/halos of other nearby galaxies. At galactocentric radii of  $R < 20 - 30$  kpc, similar to the location of our M81 pointing, the spheroid of M31 is dominated by a largely metal-rich ( $[\text{Fe}/\text{H}] \sim -0.6$ ) population (e.g., Durrell et al. 2001; Kalirai et al. 2006; Gilbert et al. 2007; Richardson et al. 2008). The stars in the halo of the Milky Way are metal-poor, with typical  $[\text{Fe}/\text{H}]$  values of  $-1.4$  to  $-1.6$  for the inner halo (out to  $\approx 10 - 15$  kpc) (Ryan & Norris 1991; Ivezić et al. 2008) and  $\approx -2.2$  beyond this (Carollo et al. 2007, and references within). The halo of the E/S0 galaxy NGC 3379 (at a galactocentric distance of 33 kpc) shows a broad metallicity distribution with a significant number of metal-poor ( $[\text{M}/\text{H}] < -0.7$ ) stars (Harris et al. 2007b). In contrast, the large elliptical galaxy NGC 5128 has a metal-rich halo with  $[\text{M}/\text{H}] = -0.6$  to  $-0.7$  at *all* locations studied thus far, from 8-38 kpc (Harris et al. 1999; Harris & Harris 2000, 2002; Rejkuba et al. 2005). Similarly, the elliptical galaxy NGC 3377 also shows a largely metal-rich population at small galactocentric radii (Harris et al. 2007a).

Taken together, large, nearby galaxies exhibit a wide diversity of halo metallicities, showing no clear trends with parent galaxy mass or morphological type (although there are suggestions that halo metallicity increases with galaxy mass, e.g., Mouhcine et al. 2006). Indeed, it appears that variations in the metallicity of halo stars *even at different locations within a given 'halo'* could make any trends with parent galaxy properties difficult to quantify. For example, the metallicity of stars in our single M81 field are similar to that of the 'halo' of NGC 3379, the 'outer halo' of M31, and the 'inner halo' of the Milky Way (assuming  $[\alpha/\text{Fe}] \sim +0.3 - 0.4$ ). If we have indeed sampled the halo of M81, an open question is whether an even more metal-poor population exists at larger galactocentric radii; again, future studies of more distant M81 field would be worthwhile.

While our CMD does not reach the main sequence turnoff region, the most reliable age-sensitive feature in the CMD, it still holds clues to the dominant age of the stars in this region of M81. Formal fits to the RC, RGB, and RGB bump give consistent estimates for the mean age of the stars of  $9 \pm 2$  Gyr. The fact that we do not observe a strong population of blue horizontal branch stars is also consistent with these results.

We can compare the ages estimated for stars in the spheroids of different galaxies, although it should be noted that these estimates come from different techniques<sup>7</sup>. The dominant population of our M81 field is

slightly younger but consistent with the mean ages (9.7, 11.0, and 10.5 Gyr, for fields at distances of 11, 21, and 35 kpc from M31) of the M31 halo fields studied by Brown et al. (2008, and references within). The halo of M31 also harbors globular clusters as old as those in the Milky Way (Alves-Brito et al. 2009; Ma et al. 2009); however, the presence or absence of any radial age trends among this population is still largely an open question.

In contrast, the stars in our M81 field appear to be slightly younger (by  $\approx 2 - 3$  Gyr, but just within the age uncertainties), than the oldest stars in the Milky Way halo (Marin-Franch et al. 2009), as our comparison with the globular cluster NGC 362 illustrated above. While there is an age spread of a few Gyr among the Milky Way GCs with the inner halo clusters being older in the mean than those of the outer halo (Dotter et al. 2009), the ages of globular clusters in M81 (estimated from integrated spectra) are indistinguishable from Galactic globular clusters (within the sizeable uncertainties Schroder et al. 2002). It should be noted that these clusters are all projected at smaller distances in M81 than the location of our field. We note that our data do *not* rule out the presence of a minority population of older stars, as ancient as the majority Galactic globular cluster system, in this region of M81.

In the case of NGC 5128, Rejkuba et al. (2005) investigated the ages of field stars at a distance of 38 kpc using the magnitude of the RC, and found that it is consistent with an old population with a mean age of  $8 \pm 3$  Gyr, very similar to the ages that we observe in the M81 halo.

Our age and metallicity results for halo stars in M81 are in broad agreement with predictions from some  $\Lambda$ CDM models (e.g., Bullock & Johnston 2005; Font et al. 2008), where the outer ( $R > 10 - 20$  kpc) halos of  $L^*$  galaxies are expected to be formed from the accreted (over a relatively long timescale) debris of somewhat lower-mass progenitor galaxies than the more metal-rich systems that (for instance) resulted in the formation of the more metal-rich Giant Southern Stream in M31 (Fardal et al. 2006, 2008; Font et al. 2008). In this scenario, the outer halos of luminous galaxies like M81 will have more metal-poor and somewhat younger combined stellar populations than that of the (slightly) older, more metal-rich inner halo/spheroid. Our results are broadly consistent with these predictions.

## 9. SUMMARY

We have presented deep photometry of a field located 20 kpc from the center of M81, believed to be dominated by halo stars. The resulting CMD, based on HST/ACS imaging, reveals a relatively blue RGB and a HB populated predominantly redward of the instability strip (i.e., a red clump). From the shape of the RGB, the magnitude of the red clump, and the location of the RGB bump, we derive a mean metallicity of  $[\text{M}/\text{H}] = -1.15 \pm 0.11$  and an age of  $9 \pm 2$  Gyr for the dominant population in this region of M81's halo. This is the lowest metallicity found for stars in any portion of M81, almost certainly because our field is more distant than any other portion of M81 studied to date. Our age and metallicity results are broadly consistent with the predictions from  $\Lambda$ CDM models, which predict lower metallicities and younger mean ages for outer halos of spiral galaxies than for inner halos. Future studies that probe the

<sup>7</sup> while different studies assume differing ages (e.g., 12 Gyr or 14 Gyr) for the 'old' populations, the effect of these differences on metallicity are small, and do not affect our general conclusions

metallicities and ages of stars even further out in the halo of M81 will allow for better constraints on the early formation of this galaxy.

A.S. and P.R.D. were supported through funds provided by NASA through grants (GO-10604.01-A and GO-10604.02.A, respectively) from the Space Telescope Science Institute, which is operated by the Association of Universities for Research in Astronomy, Incorporated, under NASA contract NAS5-26555. The authors would like to thank Andy Dolphin and Ben Williams for their assistance with the photometric reductions with DOLPHOT, and the anonymous referee for suggesting changes that improved the paper. We would also like to thank Tom Brown and Ben Williams for providing comments on earlier versions of the manuscript, as well as Michael Siegel, Min Yun, Katie Chynoweth and Mustapha Mouhcine for helpful discussions.

*Facilities:* HST.

## REFERENCES

- Abadi, M. G., Navarro, J. F., & Steinmetz, M. 2006, *MNRAS*, 365, 747
- Alves, D. R., & Sarajedini, A. 1999, *ApJ*, 511, 225
- Alves-Brito, A., Forbes, D. A., Mendel, J. T., Hau, G. K. T., & Murphy, M. T. 2009, *MNRAS*, 395, L34
- Allende Prieto, C., Beers, T. C., Wilhelm, R., Newberg, H. J., Rockosi, C. M., Yanny, B., & Lee, Y. S. 2006, *ApJ*, 636, 804
- Barker, M.K., Ferguson, A.M.N., Irwin, M., Arimoto, N., & Jablonka, P. 2009, *AJ*, in press
- Bell, E.F., et al. 2008, *ApJ*, 680, 295
- Bellazzini, M., Ferraro, F.R., & Pancino, E. 2001, *ApJ*, 556, 635
- Brown, T.M., Ferguson, H.C., Smith, E., Kimble, R.A., Sweigart, A.V., Renzini, A., Rich, R.M. & Vandenberg, D.A. 2003, *ApJ*, 592, L17
- Brown, T.M., Ferguson, H.C., Smith, E., Guhathakurta, P., Kimble, R.A., Sweigart, A.V., Renzini, A., Rich, R.M., & Vandenberg, D.A. 2005, *AJ*, 130, 1693
- Brown, T.M., Smith, E., Ferguson, H.C., Rich, R.M., Guhathakurta, P., Renzini, A., Sweigart, A.V. & Kimble, R.A. 2006, *ApJ*, 652, 323
- Brown, T. M., et al. 2007, *ApJ*, 658, L95
- Brown, T. M., et al. 2008, *ApJ*, 685, L121
- Bullock, J.S., & Johnston, K.V. 2005, *ApJ*, 635, 931
- Carollo, D., et al. 2007, *Nature*, 450, 1020
- Carretta, E., & Gratton, R. G. 1997, *A&AS*, 121, 95
- Chapman, S. C., Ibata, R., Lewis, G. F., Ferguson, A. M. N., Irwin, M., McConnachie, A., & Tanvir, N. 2006, *ApJ*, 653, 255
- Chiboucas, K., Karachentsev, I. D., & Tully, R. B. 2009, *AJ*, 137, 3009
- Dalcanton, J. J., et al. 2009, *ApJS*, 183, 67
- Davidge, T.J. 2008, *PASP*, 120, 1145
- de Blok, W. J. G., & Walter, F. 2003, *MNRAS*, 341, L39
- DeCesar, M. E., Durrell, P. R., Ciardullo, R., Hurley-Keller, D., & Feldmeier, J.J. 2004, *BAAS*, 35, 1396
- de Mello, D.F., Smith, L.J., Sabbi, E., Gallagher, J.S., Mountain, M., & Harbeck, D.R. 2008, *AJ*, 135, 548
- Dolphin, A.E. 2000, *PASP*, 112, 1383
- Dotter, A. et al. *ApJ*, submitted
- Durrell, P.R., Harris, W.E., & Pritchett, C.J. 2001, *AJ*, 121, 2557
- Durrell, P.R., DeCesar, M.E., Ciardullo, R., & Feldmeier, J.J. 2004, *IAU Symposium 217: Recycling Intergalactic and Interstellar Matter*, eds. P.-A. Duc, J. Braine, E. Brinks, 90
- Fardal, M. A., Babul, A., Geethan, J. J., & Guhathakurta, P. 2006, *MNRAS*, 366, 1012
- Fardal, M. A., Guhathakurta, P., Babul, A., & McConnachie, A. W. 2007, *MNRAS*, 380, 15
- Fardal, M. A., Babul, A., Guhathakurta, P., Gilbert, K. M., & Dodge, C. 2008, *ApJ*, 682, L33
- Ferguson, A.M.N., Irwin, M.J., Ibata, R.A., Lewis, G.F. & Tanvir, N.R. 2002, *AJ*, 124, 1452
- Ferrarese, L., et al. 2000, *ApJ*, 529, 745
- Ferraro, F. R., Messineo, M., Fusi Pecci, F., de Palo, M. A., Straniero, O., Chieffi, A., & Limongi, M. 1999, *AJ*, 118, 1738
- Ferraro, F. R., Montegriffo, P., Origlia, L., & Fusi Pecci, F. 2000, *AJ*, 119, 1282
- Fleming, D.E.B., Harris, W.E., Pritchett, C.J., & Hanes, D.A. 1995, *AJ*, 109, 1044
- Font, A. S., Johnston, K. V., Guhathakurta, P., Majewski, S. R., & Rich, R. M. 2006, *AJ*, 131, 1436
- Font, A. S., Johnston, K. V., Ferguson, A. M. N., Bullock, J. S., Robertson, B. E., Tumlinson, J., & Guhathakurta, P. 2008, *ApJ*, 673, 215
- Freedman, W.L., et al. 1994, *ApJ*, 427, 628
- Gilbert, K. M., et al. 2007, *ApJ*, 668, 245
- Girardi, L., Bressan, A., Bertelli, G., & Chiosi, C. 2000, *A&AS*, 141, 371
- Girardi, L., Bertelli, G., Bressan, A., Chiosi, C., Groenewegen, M.A.T., Marigo, P., Salasnich, B., & Weiss, A. 2002, *A&A*, 391, 195
- Guhathakurta, P., et al. 2006, preprint (astro-ph/0502366)
- Hammer, F., Puech, M., Chemin, L., Flores, H., & Lehnert, M. D. 2007, *ApJ*, 662, 322
- Harris, W. E. 2001, *Saas-Fee Advanced Course 28: Star Clusters*, 223
- Harris, G. L. H., Harris, W. E., & Poole, G. B. 1999, *AJ*, 117, 855
- Harris, G. L. H., & Harris, W. E. 2000, *AJ*, 120, 2423
- Harris, W. E., & Harris, G. L. H. 2002, *AJ*, 123, 3108
- Harris, W.E. 1990, *PASP*, 102, 949
- Harris, W.E., Harris, G.L.H., Layden, A.C., & Stetson, P.B. 2007, *AJ*, 134, 43
- Harris, W.E., Harris, G.L.H., Layden, A.C., & Wehner, E.M.H. 2007, *ApJ*, 666, 903
- Ibata, R., Irwin, M., Lewis, G., Ferguson, A.M.N. & Tanvir, N. 2001, *Nature*, 412, 49
- Ibata, R., Chapman, S., Ferguson, A. M. N., Lewis, G., Irwin, M., & Tanvir, N. 2005, *ApJ*, 634, 287
- Ibata, R., Martin, N.F., Irwin, M., Chapman, S., Ferguson, A.M.N., Lewis, G.F. & McConnachie, A.W. 2007, *ApJ*, 671, 1591
- Irwin, M. J., Ferguson, A. M. N., Ibata, R. A., Lewis, G. F., & Tanvir, N. R. 2005, *ApJ*, 628, L105
- Ivezić, Ž., et al. 2008, *ApJ*, 684, 287
- Jurić, M., et al. 2008, *ApJ*, 673, 864
- Kalirai, J.S. et al. 2006, *ApJ*, 648, 389
- Karachentsev, I.D., Karachentseva, V.E., & Borngen, F. 1985, *MNRAS*, 217, 731
- Karachentsev, I.D., et al. 2002, *A&A*, 383, 125
- Karachentseva, V.E., Karachentsev, I.D., & Borngen, F. 1985, *A&A*, 60, 213
- Klement, R., et al. 2009, *ApJ*, 698, 865
- Lee, M.G., Freedman, W.L., & Madore, B.F. 1993, *ApJ*, 417, 553
- Ma, J., Fan, Z., de Grijs, R., Wu, Z., Zhou, X., Wu, J., Jiang, Z., & Chen, J. 2009, *AJ*, 137, 4884
- Mackey, A. D., et al. 2009, *MNRAS*, in press (arXiv:0909.1456)
- Madore, B.F., & Freedman, W.L. 1995, *AJ*, 109, 1645
- Makarova, L.N., et al. 2002, *A&A*, 396, 473
- Marin-Franch, A., et al. 2009, *ApJ*, 694, 1498
- Marigo, P., Girardi, L., Bressan, A., Groenewegen, M.A.T., Silva, L., & Granato, G. L. 2008, *A&A*, 482, 883
- Maybhate, A., Masiero, J., Hibbard, J. E., Charlton, J. C., Palma, C., Knierman, K. A., & English, J. 2007, *MNRAS*, 381, 59
- McCommas, L.P., Yoachim, P., Williams, B.F., Dalcanton, J.J., Davis, M.R., & Dolphin, A.E. 2009, *AJ*, 137, 4707
- McConnachie, A.W., Irwin, M.J., Ferguson, A.M.N., Ibata, R.A., Lewis, G.F., & Tanvir, N. 2004, *MNRAS*, 350, 243
- McConnachie, A.W. et al. 2009, *Nature*, 461, 66
- Mouhcine, M., & Ibata, R. 2010, *MNRAS*, in press
- Mouhcine, M. 2006, *ApJ*, 652, 277
- Mouhcine, M., Ferguson, H.C., Rich, R.M., Brown, T.M., & Smith, T.E. 2005, *ApJ*, 633, 810
- Mouhcine, M., Rejkuba, M., & Ibata, R. 2007, *MNRAS*, 381, 873
- Mould, J., & Kristian, J. 1986, *ApJ*, 305, 591
- Newberg, H. J., et al. 2002, *ApJ*, 569, 245
- Newberg, H. J., Yanny, B., & Willett, B. A. 2009, *ApJ*, 700, L61
- Pietrinferni, A., Cassisi, S., Salaris, M., & Castelli, F. 2004, *ApJ*, 612, 168



- Rejkuba, M., Greggio, L., Harris, W.E., Harris, G.L.H., & Peng, E.W. 2005, *ApJ*, 631, 262
- Rejkuba, M., Mouhcine, M., Ibata, R. 2009, *MNRAS*, in press
- Richardson, J. C., et al. 2008, *AJ*, 135, 1998
- Riess, A. 2003, ACS ISR 2003-009 (Baltimore, STScI)
- Rizzi, L., Tully, R.B., Makarov, D., Makarova, L., Dolphin, A.E., Sakai, S., Shaya, E.J. 2007, *ApJ*, 661, 815
- Robin, A. C., Reyl  , C., Derri  re, S., & Picaud, S. 2003, *A&A*, 409, 523
- Ryan, S., & Norris, J. 1991, *AJ*, 101, 1865
- Sabbi, E., Gallagher, J.S., Smith, L.J., de Mello, D.F., & Mountain, M. 2008, *ApJ*, 676, L113
- Sakai, S., Madore, B.F., & Freedman, W.L. 1996, *ApJ*, 461, 713
- Sakai, S., & Madore, B.F. 2001, *ApJ*, 555, 280
- Sarajedini, A. 2009, in *The Ages of Stars*, IAU Symposium, Vol. 258, p. 221
- Sarajedini, A., & Jablonka, P. 2005, *AJ*, 130, 1627
- Sarajedini, A., et al. 2007, *AJ*, 133, 1658
- Sirianni, M., et al. 2005, *PASP*, 117, 1049
- Schlegel, D.J., Finkbeiner, D.P., & Davis, M. 1998, *ApJ*, 500, 525
- Schroder, L. L., Brodie, J. P., Kissler-Patig, M., Huchra, J. P., & Phillips, A. C. 2002, *AJ*, 123, 2473
- Smith, M. C., et al. 2009, *MNRAS*, 399, 1223
- Stetson, P.B. 1987, *PASP*, 99, 191
- Stetson, P.B., Davis, L.E., & Crabtree, D.R. 1990, in *ASP Conf. Ser. 8, CCDs in Astronomy*, ed. G.H. Jacoby (San Francisco:ASP), 289
- Stetson, P.B. 1992, in *ASP Conf. Ser. 25, Astronomical Data Analysis Software and Systems I*, eds. D.M. Worral, C. Biemesderfer, and J. Barnes (San Francisco:ASP), 297
- Thilker, D. A., et al. 2007, *ApJS*, 173, 538
- Tikhonov, N. A., Galazutdinova, O.A., & Drozdovsky, I.O. 2005, *A&A*, 431, 12
- Weisz, D. R., Skillman, E. D., Cannon, J. M., Dolphin, A. E., Kennicutt, R. C., Jr., Lee, J., & Walter, F. 2008, *ApJ*, 689, 160
- Williams, B.F., et al. 2009, *AJ*, 137, 419
- Yanny, B., et al. 2003, *ApJ*, 588, 824
- Yun, M.S., Ho, P.T.P., & Lo, K.Y. 1994, *Nature*, 372, 530
- Yun, M.S. 1999, *Galaxy Interactions at Low and High Redshift*, IAU Symp. 186, ed. D.Sanders, 81
- Zinn, R. J. 1985, *ApJ*, 293, 424

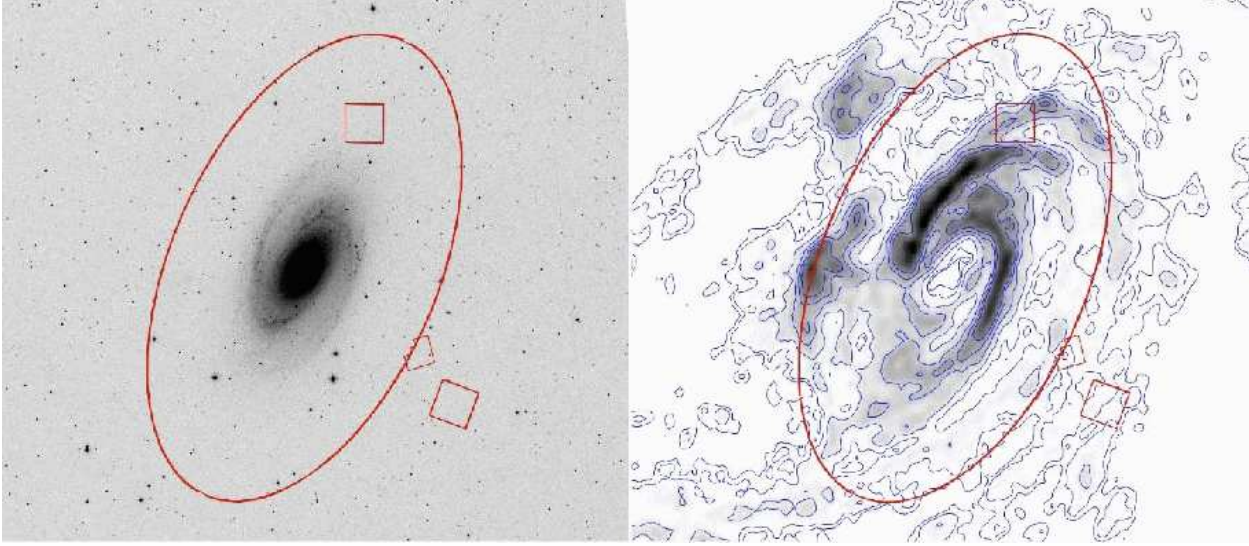


**Figure 1. (Left:)** The location and field of view of our ACS field (at lower right), superimposed on a red Digitized Sky Survey image of M81. The ACS field is located somewhat beyond the WFPC2 field of Mouchine et al. (2005), which is also shown. The ellipse indicates the  $22'$  ( $\sim 25$  kpc) extent of M81's thick disk as suggested by Tikhonov et al. (2005), inclined at  $59^\circ$ . The box at upper center is the location of the deep ACS study by Williams et al. (2009); Dalcanton et al. (2009) **(Right:)** The same thick disk and ACS field pointings as the figure on the left are shown, overplotted on the greyscale HI map of the M81 system by Yun et al. (1994), where the contours represent  $N(HI) = 0.5, 1.0, 2.5, 5.0, 7.5$  and  $10 \times 10^{20} \text{ cm}^{-2}$ . While our ACS field is superposed on some of the HI in the system, the column densities at this location are lower than that expected in order for star formation to occur. Both images are roughly  $48'$  high and  $57'$  wide; north is up, and east is to the left.

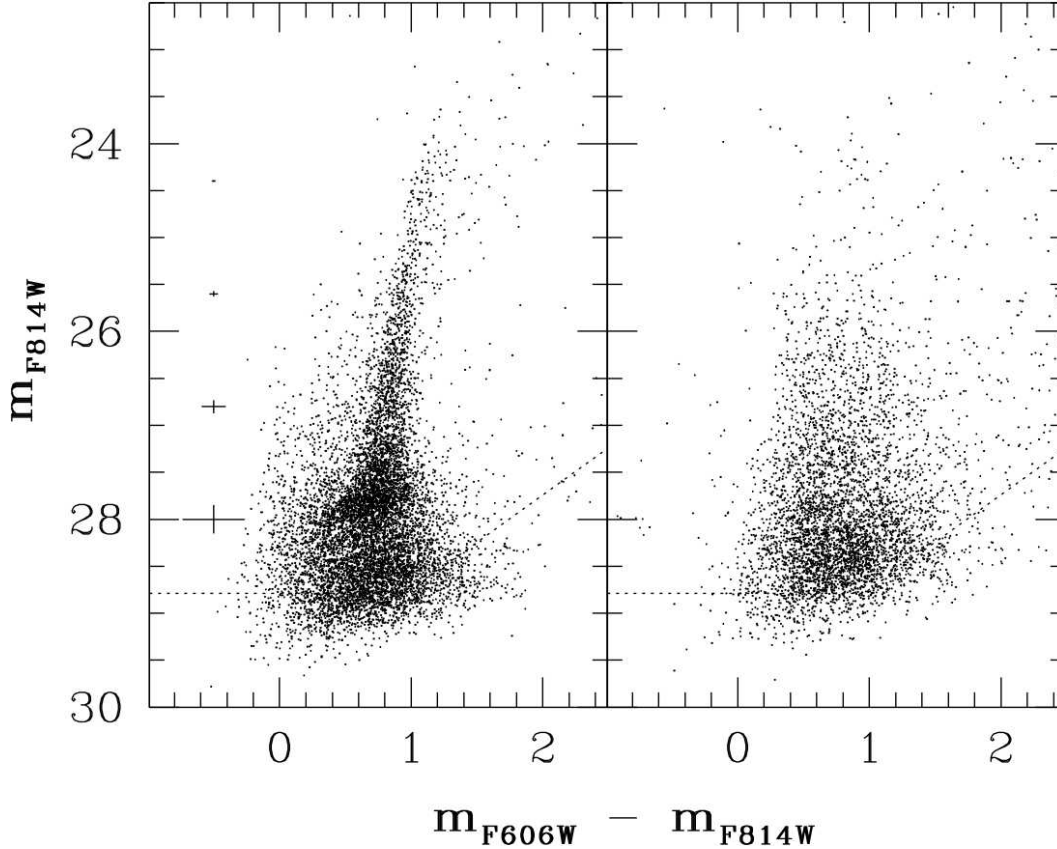


**Figure 2. (Left:)** The  $F814W$ ,  $F606W - F814W$  color-magnitude diagram for all stellar sources measured in our ACS field, after removal of objects which did not meet the selection criteria ( $\chi^2$ , sharpness, and crowding) as defined in the text. The error bars on the left denote the average errors in the photometry based on the artificial star experiments. The CMD is dominated by an old red giant branch as well as a horizontal branch/red clump at  $m_{F814W} \sim 28$ . A sequence of blue ( $m_{F606W} - m_{F814W} \sim 0$ ) objects is also seen extending upward to  $m_{F814W} \sim 26$ . **(Right:)** The CMD of all objects measured by DOLPHOT that were *rejected* by our selection criteria. The dashed lines in each figure denote the 50% completeness limits in both  $m_{F606W}$  and  $m_{F814W}$ .

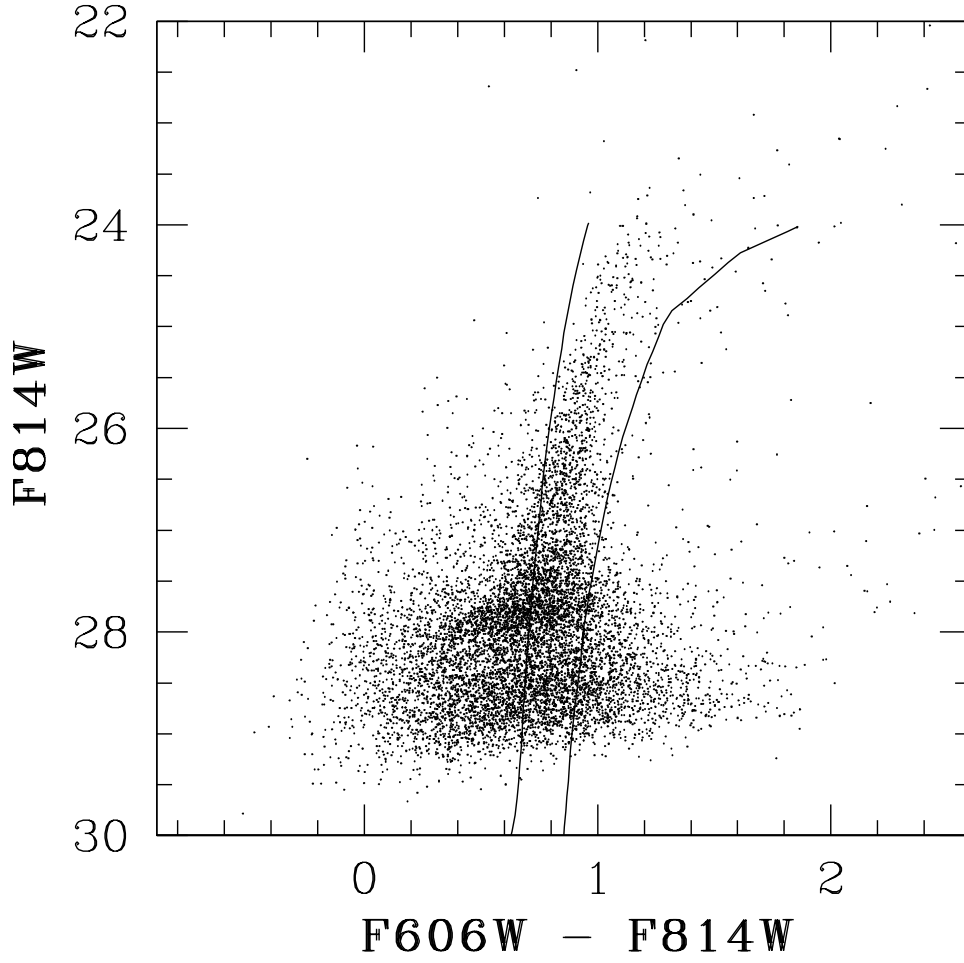


**Figure 3.** M81 halo CMD showing the loci used to define our RGB sample. The 12.6 Gyr Girardi et al. (2002)  $Z=0.0001$  (left) and  $Z=0.004$  (right) models have been shifted outward by 0.05 magnitude to account for photometric spread. The models were also shifted via a distance modulus  $(m - M)_{F814W} = 27.95$ , and reddened by  $E(F606W - F814W) = 0.08$ .

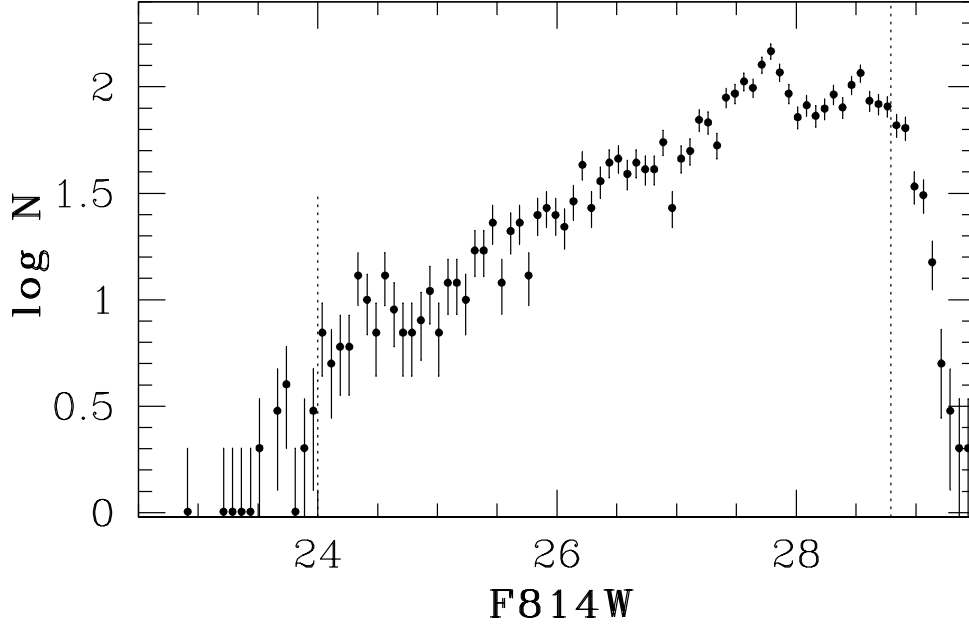


**Figure 4.**  $m_{F814W}$  luminosity function for all stars between the RGB loci in Figure 4. No corrections for photometric incompleteness have been made, nor have any (small) foreground star contributions been removed. The uncertainties are simply the  $\sqrt{N}$  statistics for the objects detected in each 0.075 mag bin. The dashed line at  $m_{F814W} = 28.79$  denotes the 50% completeness level of the photometry. The solid line at  $m_{F814W} = 24.00$  represents the location of the RGB tip.

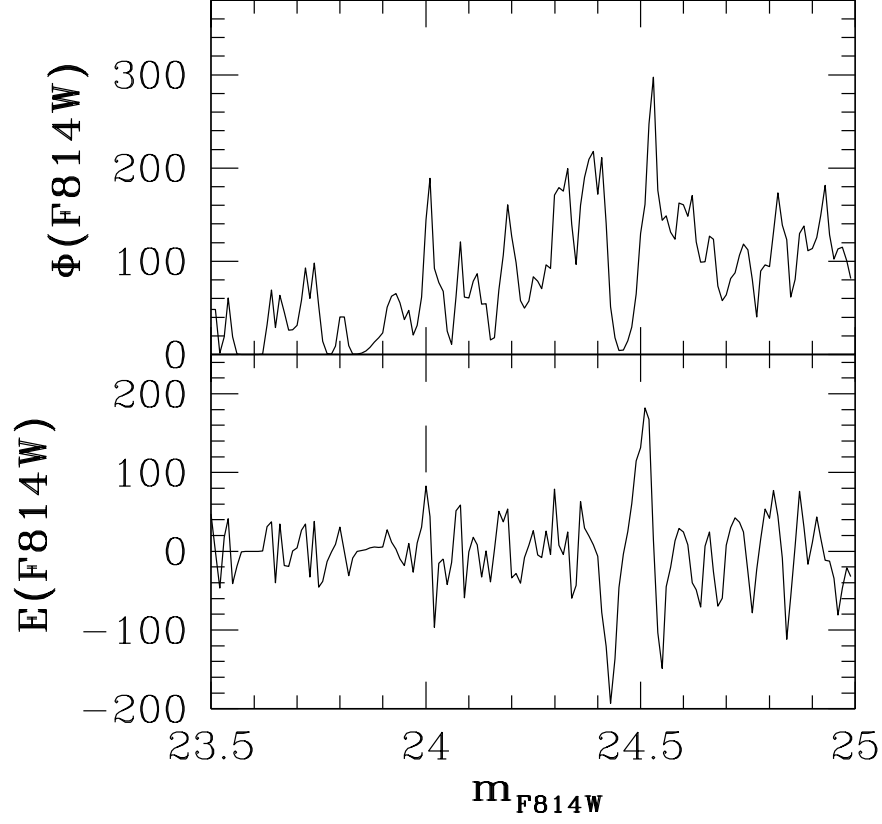


**Figure 5.** The top panel shows a smoothed luminosity function formed by co-adding the Gaussian representation of stars in our RGB subsample (see text). The bottom panel is the result of applying the Sobel edge-detection algorithm. The peak at  $m_{F814W, RGB} = 24.00 \pm 0.02$  (internal error only) is the most likely location of the RGB tip.

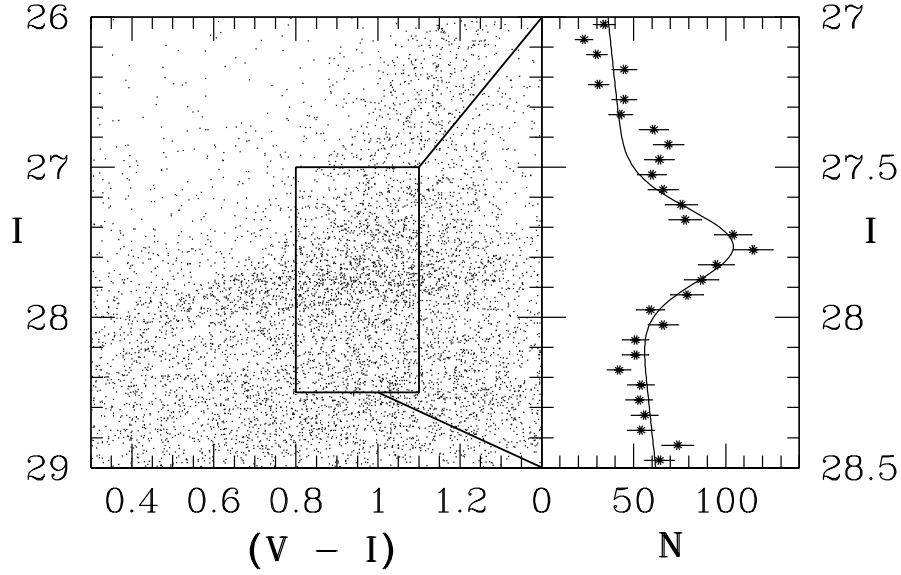


**Figure 6.** **(Left:)** A close up of the region around the red clump and horizontal branch in the  $I$ ,  $V - I$  color-magnitude diagram (transformed from the ACS magnitudes using the Sirianni et al. (2005) transformations – see text). The box illustrates the region within which the red clump magnitudes have been derived. **(Right:)** The binned  $I$  band luminosity function for objects within the boxed region. The LF has not been corrected for photometric incompleteness. The solid line shows the combined linear background and best-fit Gaussian to the location of the red clump, at  $I = 27.76 \pm 0.04$ , and a dispersion  $\sigma = 0.12^{+0.04}_{-0.03}$ .

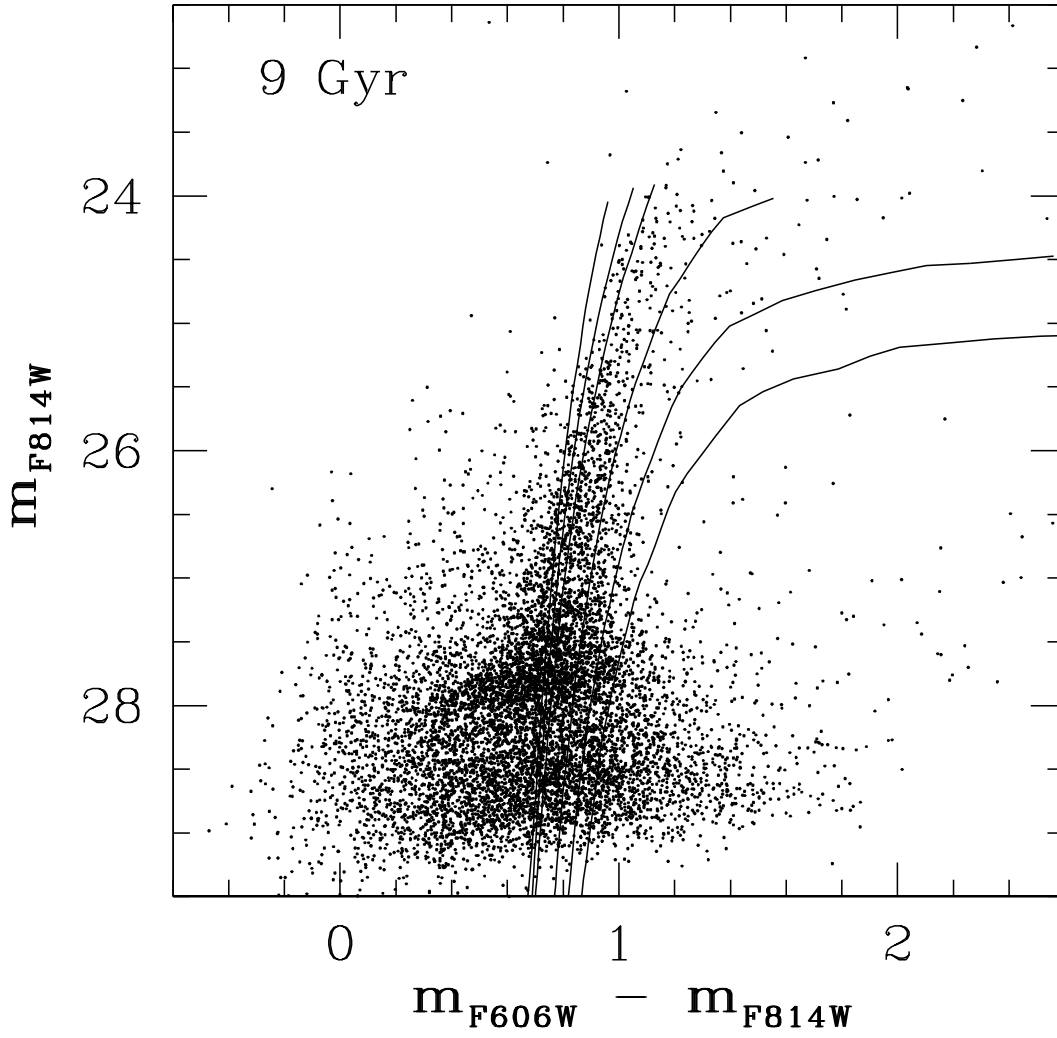


**Figure 7.** Our M81 field CMD overplotted with the 9 Gyr RGB models from Marigo et al. (2008), for metallicities of (from left to right)  $[M/H] = -2.3, -1.7, -1.3, -0.7, -0.4, 0.0$ . All models have been shifted by  $E(F606W - F814W) = 0.08$  and  $(m - M)_{F814W} = 27.95$ .

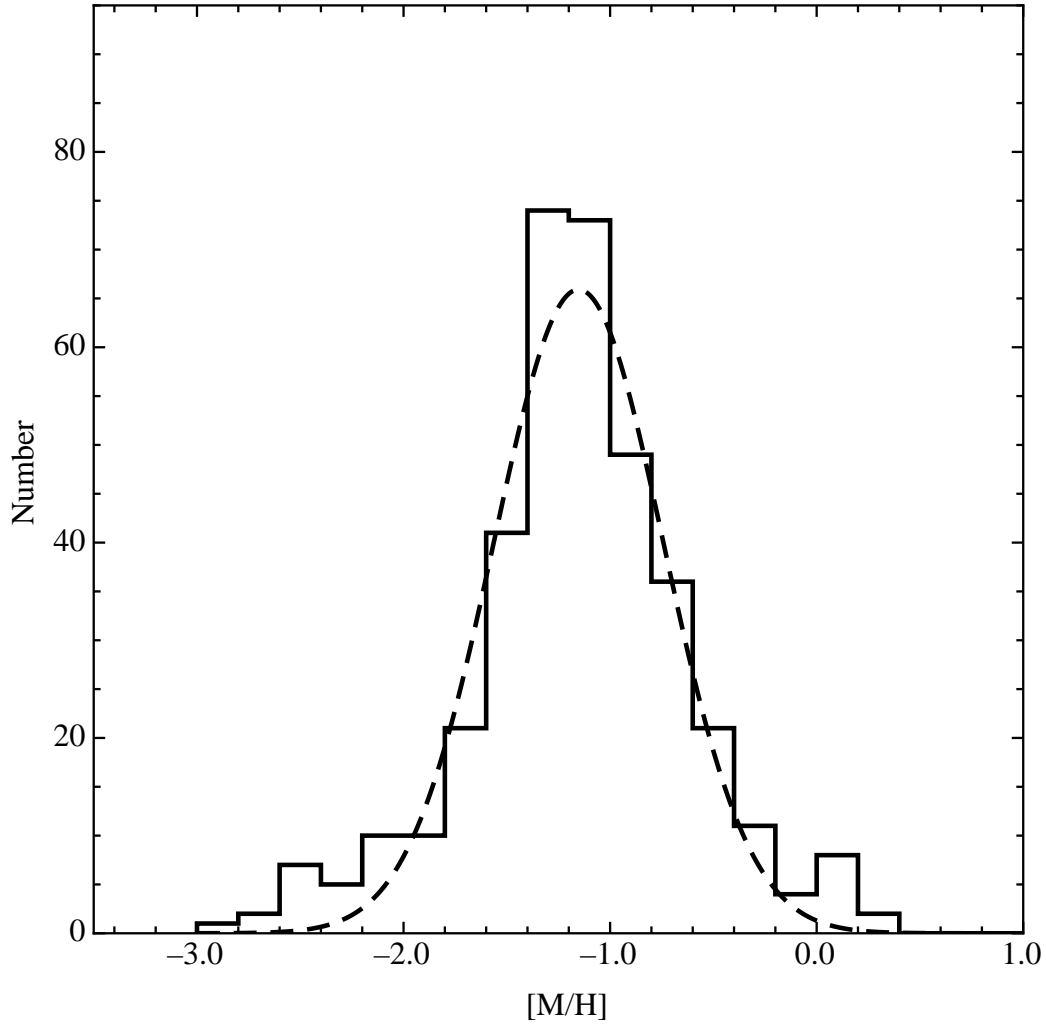


**Figure 8.** A plot of the derived metallicity distribution function for stars in our M81 field. The solid line is the binned histogram of metallicity determinations for RGB stars with  $M_I < -2.0$  using the Girardi et al. (2000) isochrones (see text). The dashed line is the Gaussian fit to the core of this distribution. We assume an age of  $\log(\tau/\text{yr}) = 9.95$ .



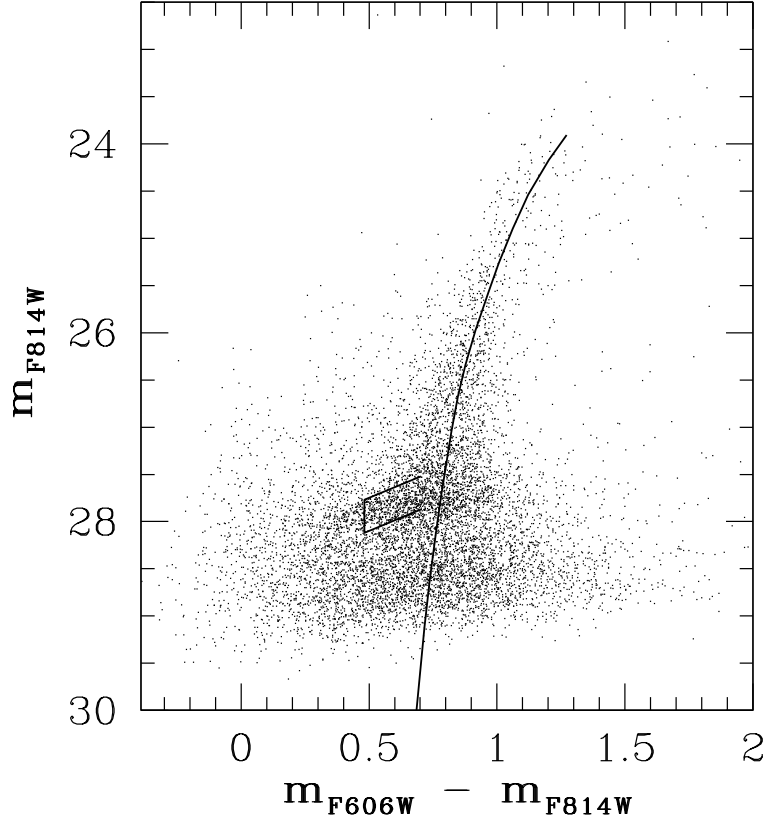


**Figure 9.** The CMD of our M81 halo field, overplotted with the fiducial of the Milky Way globular cluster NGC 362 from the HST Treasury project, and the bounding box of the red HB. The fiducial has been shifted by  $\Delta(m_{F606W} - m_{F814W}) = 0.05$  and  $\Delta m_{F814W} \sim \Delta I = 13.12$  to match the distance and reddening of M81.

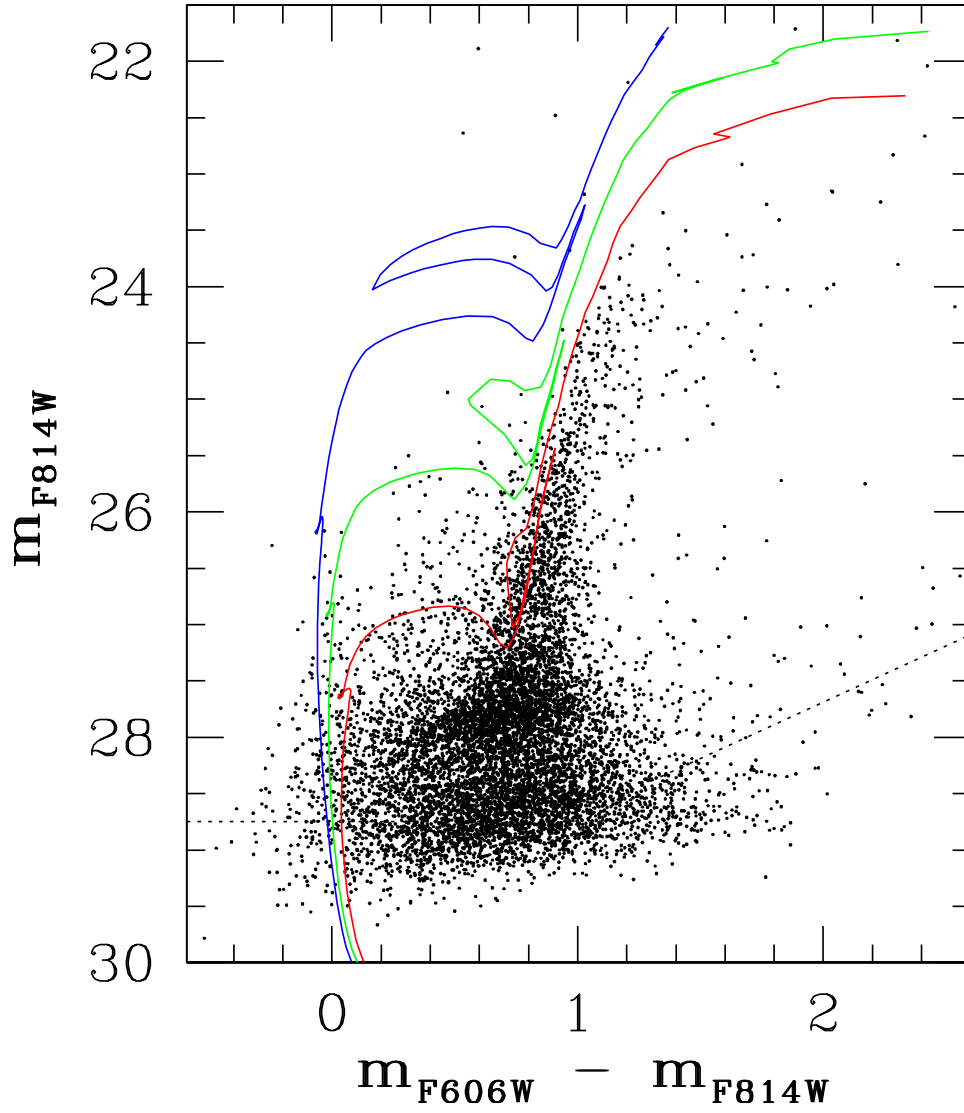


**Figure 10.** Our M81 field CMD overplotted with  $Z=0.008$  isochrones from Marigo et al. (2008). The ages are (from top to bottom) 100 Myr, 200 Myr, 400 Myr. As before, all models have been shifted by  $E(F606W - F814W) = 0.08$  and  $(m - M)_{F814W} = 27.95$ .

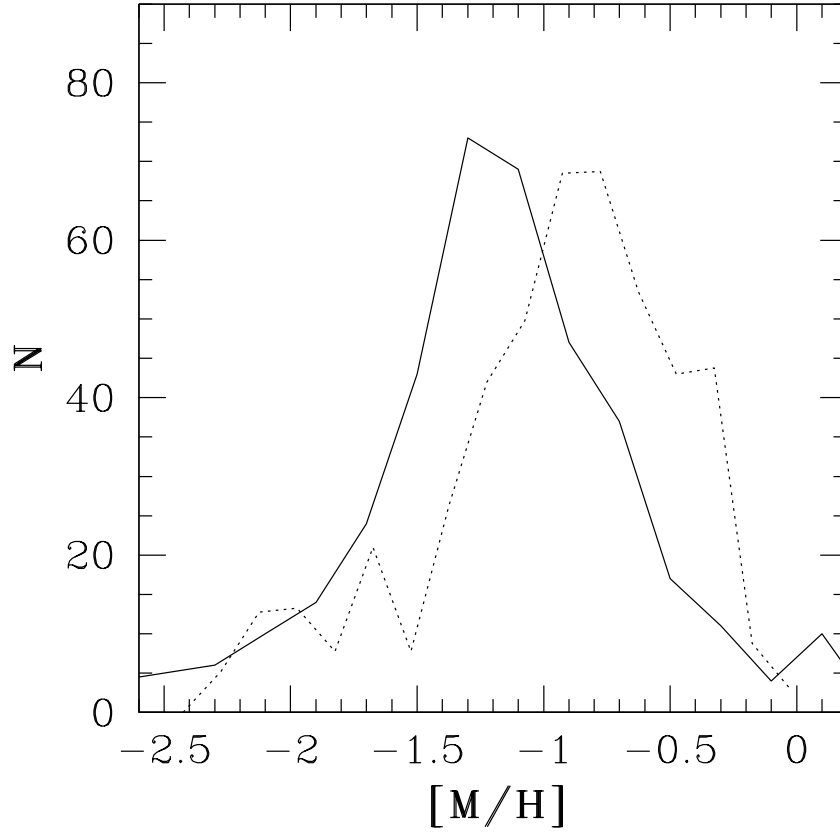


**Figure 11.** Comparison between our MDF (for an age of 9 Gyr) [solid line] and that of the MDF of an interior field from Mouchine et al. (2005) (for an assumed age of  $\sim 12$  Gyr; dashed line)